Start Clim 2024

Analyse der Auswirkungen von Hitzeperioden auf die Oberflächen- und Wassertemperatur in der Region Neusiedler See - Seewinkel mit thermischen Satellitendaten (HOT)

Projektmitarbeiter*innen und Autor*innen des Berichtes:

Vanessa Streifeneder, Arellano Carla Mae, Zahra Dabiri, Daniel Hölbling

PARIS
LODRON
UNIVERSITY
SALZBURG

Z GIS

Inhaltsverzeichnis

Abbildungsverzeichnis

Tabellenverzeichnis

A-1 Kurzfassung

Der Neusiedler See ist einer der wenigen Steppenseen Europas und bildet mit seinem salzhaltigen Wasser, den Salzlacken und dem ausgedehnten Schilfgürtel ein einzigartiges Ökosystem. Aufgrund des pannonischen Klimas ist die Region die wärmste Österreichs. Der See wird hauptsächlich durch Niederschläge gespeist, die nahen Salzlacken trocknen regelmäßig aus. Extremereignisse wie Hitze und Dürre – zunehmend durch den Klimawandel verstärkt – gefährden das fragile Ökosystem. Das Projekt HOT untersuchte die Auswirkungen zunehmender Hitzewellen auf Land- und Wasseroberflächen anhand frei verfügbarer thermischer und optischer Satellitendaten. Zeitreihenanalysen wurden durchgeführt, um Temperaturtrends, Vegetationsveränderungen und Unterschiede zwischen Schutzgebieten und nicht geschützten Flächen zu analysieren. Die Kombination von Satelliten- und meteorologischen Daten erlaubt ein flächendeckendes Monitoring der Oberflächen- und Wassertemperatur sowie der Vegetationsvitalität – ein wichtiger Beitrag zur Bewertung von Klimawandelfolgen und zur Entwicklung von Regenerations- und Managementstrategien.

Zwischen 1982 und 2024 zeigt die Region Neusiedler See einen Anstieg in Häufigkeit und Dauer von Hitzewellen, die inzwischen früher im Jahr beginnen und später enden – was die Bedeutung einer kontinuierlichen räumlich-zeitlichen Überwachung unterstreicht. Analysen von Vegetationsindizes und Oberflächentemperaturen belegen, dass geschützte und ungeschützte Gebiete unterschiedlich auf Hitzewellen reagieren. Dies ist abhängig von der Landnutzung wie auch von der Hitzewelle selbst. Landwirtschaftlich genutzte Flächen sind eher in ungeschützten Gebieten vertreten und können durch das Eingreifen der Bauern und eine angepasste Fruchtfolge oft weniger anfällig für Hitzewellen sein als lokale geschützte Ökosysteme mit weniger hitzeresistenten Pflanzen, die nicht an ein geringeres Niederschlagsregime oder erhöhtes Evaporationsregime angepasst sind.

A-2 Abstract

Lake Neusiedl is one of the few steppe lakes in Europe and, with its saline water, salt pans, and extensive reed belt, forms a unique ecosystem. Due to the Pannonian climate, the region is the warmest in Austria. The lake is mainly fed by precipitation, and the nearby salt pans regularly dry out. Extreme events such as heat and drought – increasingly intensified by climate change – pose a threat to this fragile ecosystem.

The HOT project examined the effects of increasing heatwaves on land and water surfaces using freely available thermal and optical satellite data. Time series analyses were conducted to investigate temperature trends, vegetation changes, and differences between protected and non-protected areas. The combination of satellite and meteorological data allows for comprehensive monitoring of surface and water temperatures as well as vegetation vitality – an important contribution to assessing the impacts of climate change and developing regeneration and management strategies.

Between 1982 and 2024, the Neusiedler See region shows an increase in the frequency and duration of heatwaves, which now begin earlier in the year and end later – highlighting the importance of continuous spatio-temporal monitoring. Analyses of vegetation indices and surface temperatures show that protected and non-protected areas respond differently to heatwaves. This depends both on land use and the nature of the heatwave itself. Agricultural areas are more often located in non-protected zones and, due to farmer intervention and adapted crop rotation, are often less vulnerable to heatwaves than local protected ecosystems, which may contain less heat-resistant plant species not adapted to a reduced precipitation or increased evapotranspiration regime.

A-3 Methods to analyse heatwaves with Earth observation data

Earth observation (EO) data facilitates the detection, monitoring, and assessment of heatwave events and their impacts on the environment over space and time. Thermal infrared sensors aboard satellites such as MODIS, Landsat, and Sentinel-3 provide land surface temperature (LST) data, which can be used to identify surface temperatures over wide areas and for different land cover types. Time series analysis helps track temperature trends and anomalies, while vegetation indices derived from optical satellite imagery offer insights into the impacts of heatwaves on ecosystems. Combining satellite data with meteorological observations enhances our understanding of heatwave dynamics, spatial extent, and potential risks to human and environmental health.

Wegler & Kuenzer (2024) reviewed the potential of different EO data to detect the impacts of climate change and extreme weather events on forests. The authors found that primarily optical satellite data are used, while only a few studies have used thermal data or combined different sensor types. Vegetation indices derived from EO data have been successfully applied to assess drought stress and heatwave impacts (Crocetti et al., 2020; Richter et al., 2008). However, many studies focus only on single indices, such as the Normalized Difference Vegetation Index (NDVI), and do not integrate satellite-derived LST data.

LST derived from thermal EO data is a geophysical variable that reflects the surface energy balance and plays a crucial role in monitoring climate dynamics, vegetation stress, and evapotranspiration (Li et al., 2013). As a fundamental component of land-atmosphere interactions, LST has been applied in research on droughts, heatwaves, and land degradation. Nevertheless, despite its importance, LST remains underutilised in ecological monitoring, largely due to limitations in spatial resolution, cloud interference, and data continuity (Crocetti et al., 2020).

A-4 Study area and data acquisition

A-4.1 Study area

The Neusiedler See (English: Lake Neusiedl; Hungarian: Fertő tó), primarily located in Burgenland, Eastern Austria, with a portion extending into Hungary, is one of the few steppe lakes in Europe. Its shallow brackish water with moderate salinity, the surrounding salt marshes and salt ponds in the Seewinkel region, and the second-largest reed belt in Europe form a unique ecosystem (Nationalpark Neusieder See - Seewinkel, 2025; Zulka et al., 2022). The area is characterised by a Pannonian climate, making it the warmest region in Austria (Nationalpark Neusieder See - Seewinkel, 2025). The lake is primarily fed by rainwater, and depending on the weather, the salt ponds around Neusiedler See regularly dry out (Amon, n.d.). This unique landscape is protected under multiple conservation frameworks, including Natura 2000, the FFH (Flora-Fauna-Habitat) Directive and the Ramsar Convention (Amon, n.d.). Additionally, the Neusiedler See, its reef belt, protected areas, and 20 surrounding municipalities, were designated as a UNESCO World Heritage Site in 2001 (Tourismusverband Nordburgenland, n.d.).

This vulnerable ecosystem is increasingly threatened by extreme events such as heatwaves and droughts, which are intensified by climate change. Climate scenarios predict rising temperatures and decreasing precipitation, leading to longer drought and heat periods, lower water levels, and increased water and surface temperatures. These climatic shifts impact water quality and jeopardise native flora and fauna through drought damage, species extinction, and altered nutrient and salt balances. Therefore, continuous and comprehensive monitoring of surface and water temperatures is crucial to better understand the impact of heatwaves on the Neusieder See - Seewinkel region, evaluate management effectiveness, and develop regeneration strategies. In particular, comparing protected and non-protected areas can yield valuable insights into their differing responses to climate change and human influence. The use of thermal satellite data, with its extensive spatial coverage, offers an important complement to in-situ measurements and helps provide a more comprehensive understanding of ecosystem changes.

The study site in HOT includes only areas within Austrian borders, primarily focusing on the Neusiedler See – Seewinkel National Park, selected areas outside the national park, and areas around five weather stations. Abb. A-1: illustrates the different study sites. A buffer zone of 1.5 km was applied around each weather station. Additionally, the national park area was divided into five distinct sections to account for varying landscape characteristics. Five further locations outside the park were also selected to analyse the impact of heatwaves on non-protected areas. These sites were chosen based on their diverse landscape features. By incorporating multiple smaller study sites and integrating land cover information, the project also partially addresses the effect of irrigation.
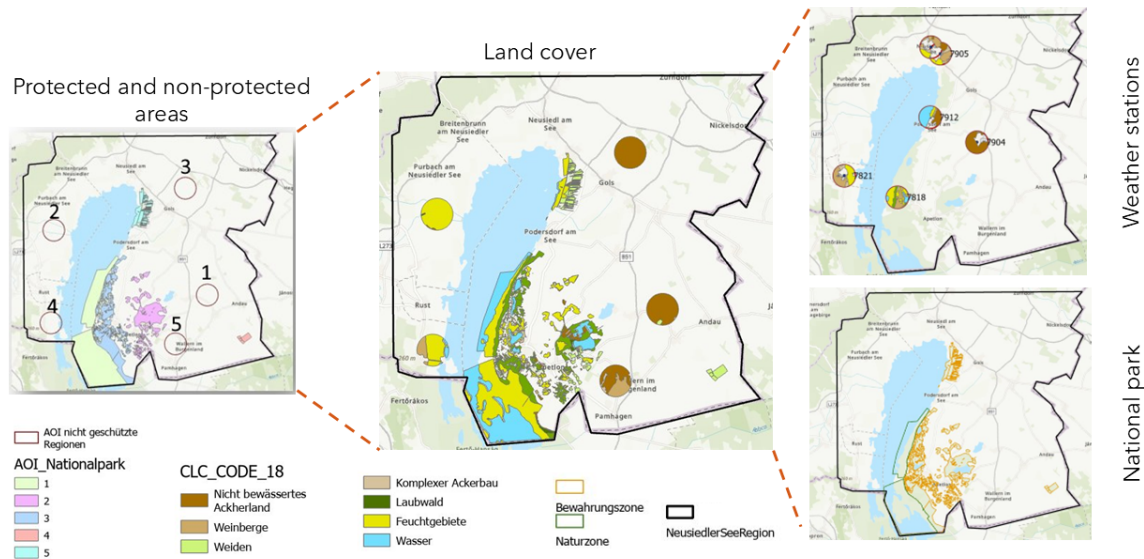
Abb. A-1: Study area Neusiedler See - Seewinkel with the selected areas for further analysis.

A-4.2 Data

For this project, we used different data sources containing meteorological and satellite data.

CORINE Land Cover 2018 (European Environmental Agency, 2018): Land cover and land cover data provided by the EU Copernicus Mission with a resolution of 100*100m for Europe.

Geosphere - Klimaindizes v2.1 Jahresdaten (GeoSphere, 2024): Rasterised dataset containing different climate indices based on the SPARTACUS project, with a resolution of 1*1km.

Geosphere Austria – WINFORE (GeoSphere, 2025c): This is a dataset containing the climatic water balance - Standardized Precipitation Evapotranspiration Index (SPEI).

Geosphere Austria – Severe Weather Archive (GeoSphere, 2025b): The severe weather archives are made available through the VIOLA web service and standardise the data collection of Geosphere Austria. Here, hail events are listed by districts and municipalities, along with information about the damage caused. These data come from Geosphere Austria itself, the European Severe Storms Laboratory (ESSL), the European Meteorological Network (EUMETNET), and newspaper articles.

Geosphere Austria (formerly ZAMG) – Station Data (GeoSphere, 2025a): The freely available station data provide daily and hourly information on temperature, precipitation, sunshine hours, etc. at the respective stations.

Water Authority Burgenland: In situ water temperature data of the Neusiedler See.

Freely available optical Sentinel-2 (S2) satellite images from the European Union's Copernicus Earth observation program were used, featuring a spatial resolution of 10 meters and a maximum temporal resolution of 5–6 days. The data was obtained using Google Earth Engine (GEE). GEE is a cloud-based service, providing access to pre-processed S2 images and the opportunity to directly calculate vegetation indices for predefined areas.

Landsat 8 Level-2 Surface Temperature (L8): The thermal infrared data (Band 10) from Landsat 8 Collection 2 was processed on GEE to retrieve LST at 100 m spatial resolution. Using NDVI-based emissivity correction, surface temperatures were derived from brightness temperature products. Cloud masking and temporal filtering were applied to ensure consistency. The resulting maps were used to analyze LST spatial patterns of the AOI.

ECOSTRESS Level 2 Land Surface Temperature: The ECO_L2T_LSTE V002 product was acquired via NASA AppEEARS, providing ~70 m resolution LST data from the International Space Station. The processed ECOSTRESS product was used to capture higher resolution spatial thermal patterns around the AOI and to support the values derived from L8.

A-5 Identifying and characterising heatwaves

To better understand the occurrence of heatwaves and to further assess the relationship between heatwaves, surface temperature, and vegetation health, a thorough analysis of heatwaves in the study areas was conducted. Selected heatwaves were additionally characterised based on temperature, precipitation and the SPEI30 time series, and potential trends were analysed. The Standardized Precipitation Evapotranspiration Index (SPEI) can be used to estimate the climatic water balance, which is the difference of precipitation and potential evapotranspiration. SPEI30 describes the climatic water balance of the last 30 days (GeoSphere, 2024).

A heatwave was defined as a period of at least three consecutive hot days, where a hot day is defined as a day with a maximum temperature of at least 30°C (GeoSphere, 2024). Additionally, we analysed the development of the number of Kysely days since 1960. Kysely days refer to the annual number of days that fall within a heatwave. According to this definition, a heatwave occurs when the daily maximum temperature (TX) exceeds 30°C for at least three consecutive days and continues as long as the average TX over the entire period remains above 30°C, with no day dropping below 25°C.

A-5.1 Trend analysis

Since the 1980s, an increase in the frequency of heatwaves has been observed in the study area Abb. A-2:. The highest number of heatwaves per year was recorded in 2012 and 2023. In most years, at least one heatwave occurred. This trend is further supported by an increase in the number of Kysely days since 1980 (Abb. A-5:).

Although heatwaves have usually occurred in July and August, since 2000 they have also been observed as early as April and May, and as late as September (Abb. A-3:). This temporal shift is likely attributable to a general rise in regional temperatures associated with climate change. (Chimani et al., 2016).

Furthermore, the data indicate an increasing duration of heatwaves since 2000, suggesting not only earlier onset but also prolonged periods of extreme heat (Abb. A-4:).
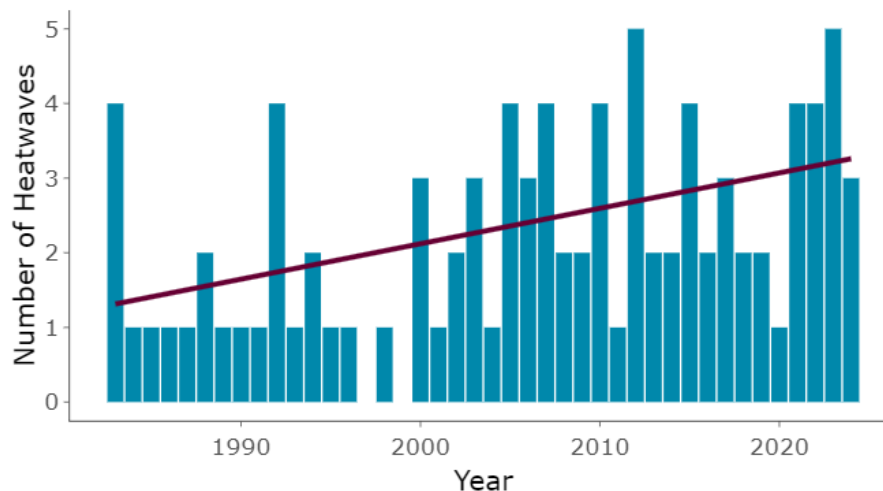
Abb. A-2: Counted heatwaves per year from 1982 until 2024. For the years 1987 and 1999, no data were available.
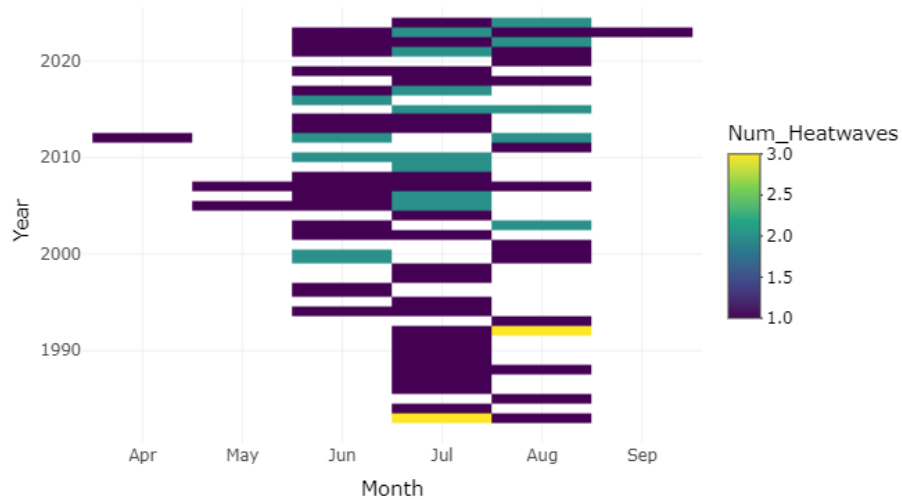
Abb. A-3: Counted heatwaves by year and month from 1982 until 2024.
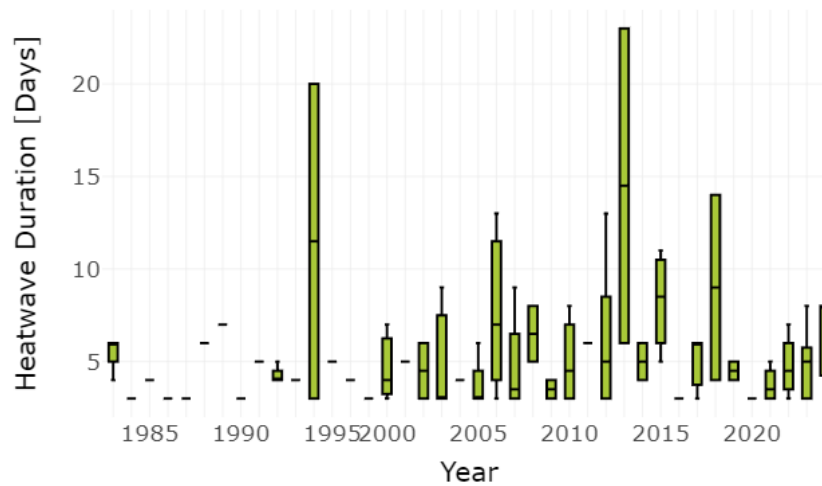
Abb. A-4: Heatwave duration distribution by year from 1982 until 2024.
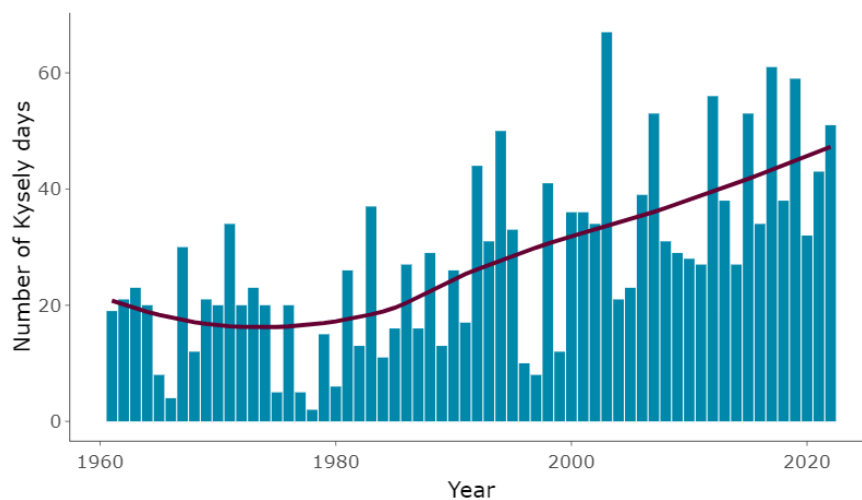
Abb. A-5: Number of Kysely days averaged over the study area from 1960 until 2024.

StartClim2024.A

For further understanding the impact of reported heatwaves in the study area, we reviewed the VIOLA archive provided by the GeoSphere Austria. From 2014 onward, only three heatwaves have been associated with reportable damage (Tab. A-1:). For example, the heatwave in 2022 led to increased fish mortality in Lake Neusiedl, attributed to water temperatures exceeding 30 °C.

Tab. A-1: Heatwaves listed in the VIOLA archive (GeoSphere, 2025b).

Start Date	End Date	Location	Description
08.07.2021	08.07.2021	Siegendorf im Burgenland, Halbtrun, Pandorf	Fire caused by a heatwave
19.07.2022	23.07.2022	Illmitz, Weiden am See, Neusiedler See	High temperature led to fish dying (over 30°C water temperature)
08.08.2024	08.09.2024	Burgenland, Purbach am Neusiedler See; Rechnitz, Südburgenland	Continuous heat period with an increasing number of tropical nights: health issues for people, dry period for agriculture, fires

A-5.2 Characterisation of selected heatwaves

For the vegetation analysis presented in A-7, we used Sentinel-2 data, which have been available since 2015. To investigate potential vegetation changes associated with heatwaves during this period, eight distinct heatwave events were selected (Tab. A-2:). Each selected heatwave had a minimum duration of one week to ensure the availability of sufficient satellite imagery. Additionally, due to the project's temporal constraints and resources, selecting more than eight events for analysis was not feasible.

Of the eight heatwaves, three occurred in 2015, and one each in 2018, 2022, and 2023, with two in 2024. The highest maximum temperature was recorded in July 2015, reaching approximately 37 °C. In contrast, the events in August 2015, 2018, and 2024 showed maximum temperatures around 30 °C.

Tab. A-2: Selected heatwaves from 2015 to 2024.

ID	Start Date	End Date	Duration	Max. Temperature
1	01.07.2015	08.07.2015	7	37.5
2	15.07.2015	25.07.2015	10	37.4
3	04.08.2015	15.08.2015	11	36.8
4	27.07.2018	10.08.2018	14	30.6
5	19.07.2022	26.07.2022	7	34.5
6	19.08.2023	27.08.2023	8	31.6

| 7 | 10.08.2024 | 18.08.2024 | 8 | 35.5 |
| 8 | 28.08.2024 | 05.09.2024 | 8 | 35 |

To better understand the conditions before and after a heatwave, we analysed a period spanning one week before each heatwave and three weeks following it. This timeframe is intended to capture potential mid-term impacts on vegetation, as well as to assess pre-heatwave conditions.

Abb. A-6: and Abb. A-7: illustrate temperature and precipitation patterns before, during, and after the selected heatwaves. No consistent trend is apparent across the events.

The following subchapters provide a more detailed characterisation of the selected heatwaves.
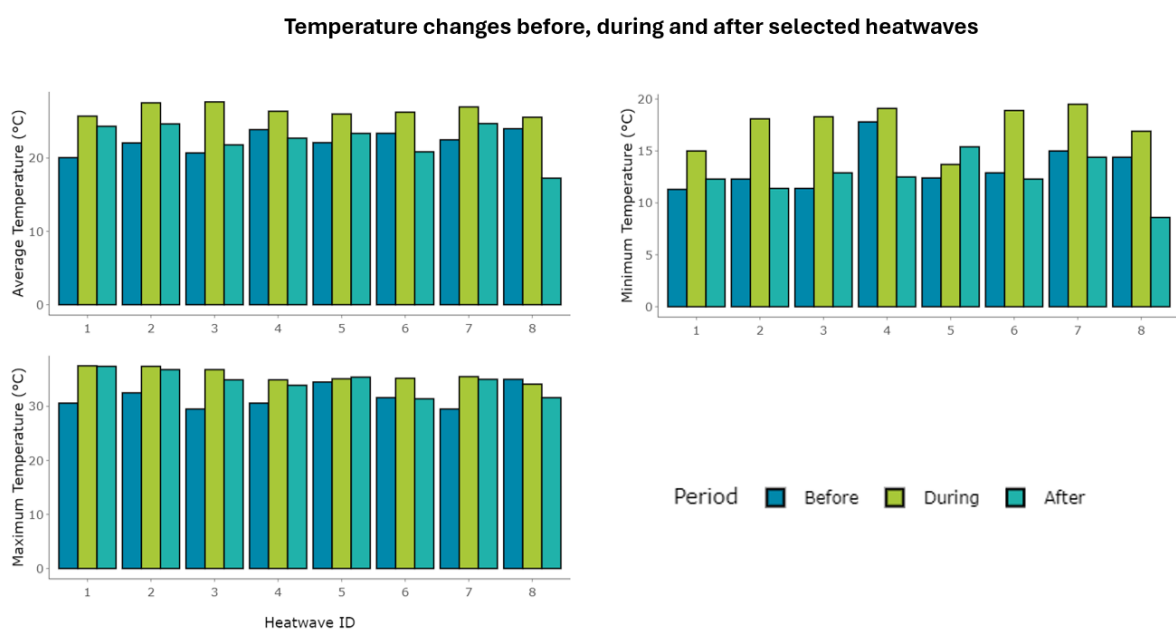
Abb. A-6: Minimum, maximum and average temperature changes before (1 week), during and after (3 weeks) selected heatwaves.
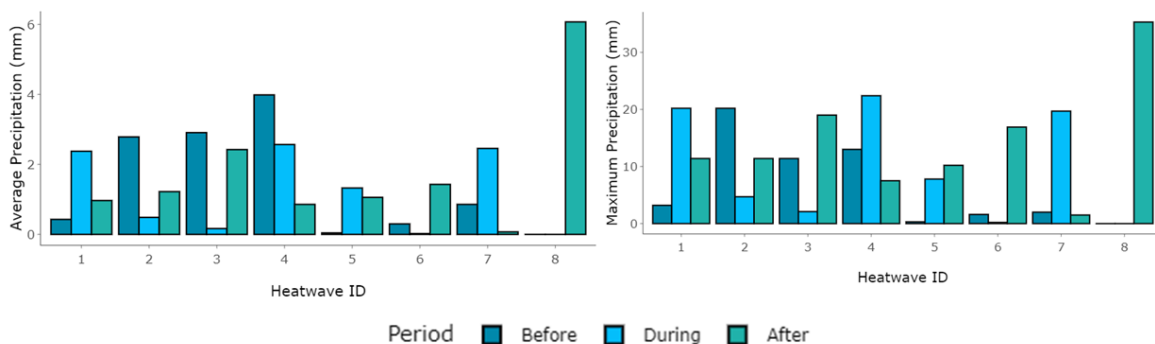
Abb. A-7: Maximum and average precipitation changes before (1 week), during and after (3 weeks) selected heatwaves.

A-5.2.1 Heatwaves in 2015

The three heatwaves in 2015 took place from the beginning of July until mid-August, with some colder days in between (Abb. A-8:). Heatwave (HW) 1 lasted one week, while HW 2 and HW 3 lasted over ten days. The average temperature during the whole duration, except for two days, was under 30°C, indicating cooler nights. When comparing the average temperature during the heatwaves with the temperature during the other days, a similar pattern of increased temperatures can be seen.

Abb. A-8: Maximum and average temperature in the time of the selected heatwaves in 2015.

Abb. A-9: shows the precipitation in the time of the heatwaves in 2015. For HW 1 and HW 3, no precipitation was detected during the heatwaves, but afterwards. In case of HW 2, some smaller rainfall events occurred during the heatwave, probably thunderstorms.
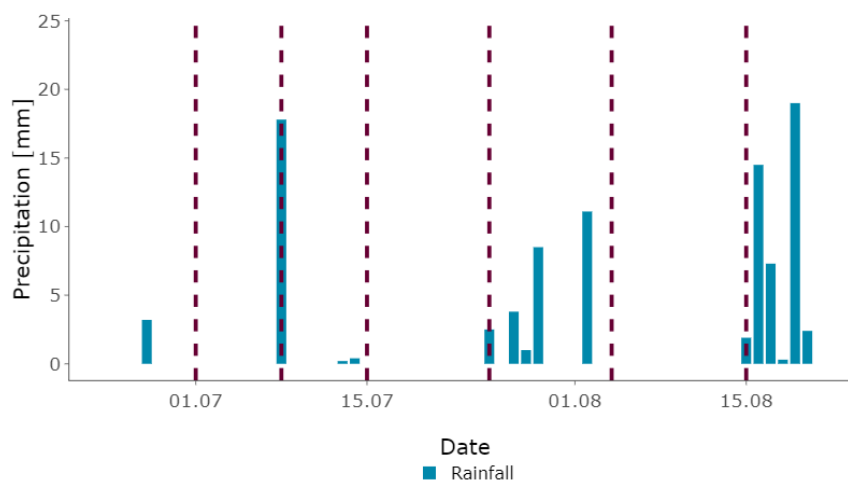
Abb. A-9: Precipitation in the time of the selected heatwaves in 2015.

The SPEI30 shows a negative range before the heatwave (-1.37 to -1.22), indicating dry conditions. During the heatwave, the index still showed dry conditions, with a slight increase to the pre-heatwave conditions (-0.99 to -0.75), probably due to the rainfall between the heatwaves. In the three weeks after the last heatwave, the index increased slightly (-0.36 to 0.02), indicating a normalisation of the water balance but no wetter conditions.

A-5.2.2   Heatwave 2018

In 2018, the selected heatwave took place at the beginning of August and had a maximum temperature of 30.6°C, whereas the average temperature stayed below 30°C (Abb. A-10:). Looking at the precipitation in Abb. A-11:Abb. A-10:, rainfall events have been detected before, during and after the heatwave with max. 20mm.

Abb. A-10: Maximum and average temperature in the time of the selected heatwave in 2018.
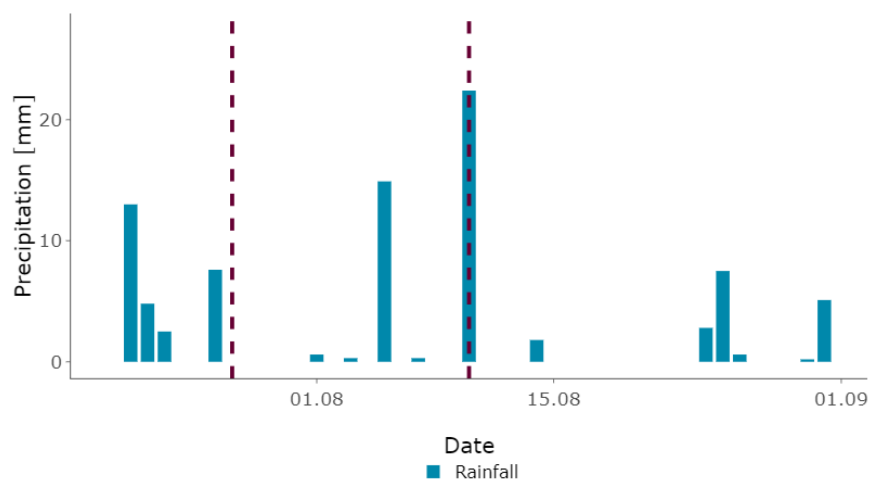
Abb. A-11: Precipitation in the time of the selected heatwave in 2018.

The SPEI30 index for 2018 shows wet conditions for the time before the heatwave (-0.06 to 0.71). This also correlates with the rainfall shown in Abb. A-11:. For the time during the heatwave, the index indicates dry conditions (-0.46 to -0.09), although some rainfall can be seen. Still, after the heatwave, there is a negative increase in the water balance (-1.18 to -0.79).

A-5.2.3   Heatwave 2022

In 2022, the selected heatwave took place at the end of July with a maximum temperature of 34.5 °C and an average daily temperature under 30°C (Abb. A-12:). At the end of the heatwave, precipitation events with a max. of 10mm rainfall have been observed. Before the heatwave, only a small precipitation event occurred, whereas five events have been recorded in the three weeks afterwards (Abb. A-13:).
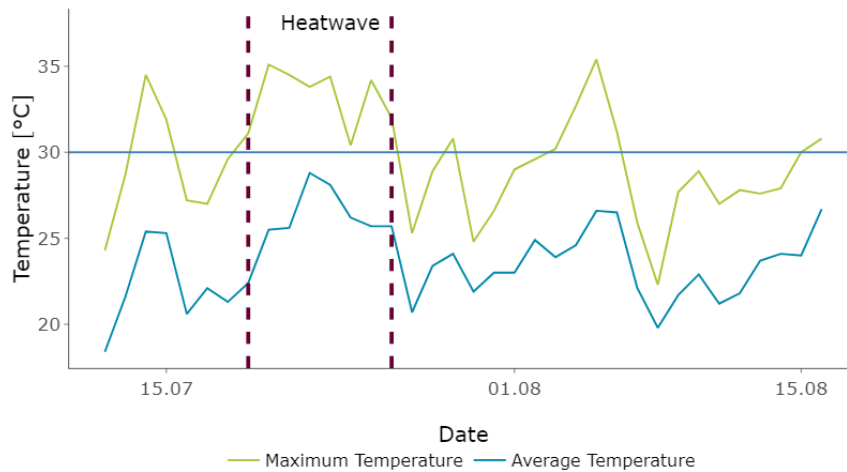
Abb. A-12: Maximum and average temperature in the time of the selected heatwave in 2022.
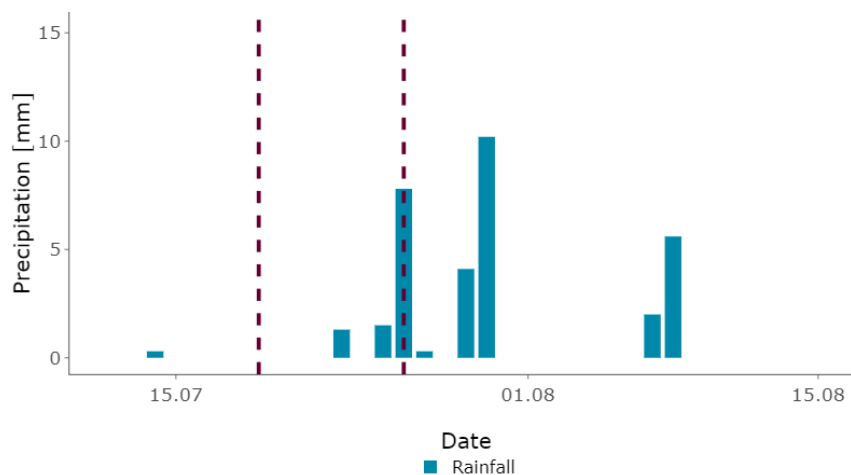
Abb. A-13: Precipitation in the time of the selected heatwave in 2022.

The SPEI 30 index indicates dry conditions already before the heatwave in 2022 (-1.53 to -1.19), which increased during the heatwave (-1.81 to -1.61). Due to the rainfall in the time after the heatwaves, the index increased (-1.14 to-0.7), although still indicating dry conditions.

A-5.2.4   Heatwave 2023

The selected heatwave in 2023 took place mid of August with a maximum temperature of 31.6°C and an average temperature between 25°C and 28°C (Abb. A-14:). During the heatwave, a small precipitation event with 2mm took place, before and afterwards further rainfall events have occurred (Abb. A-15:).
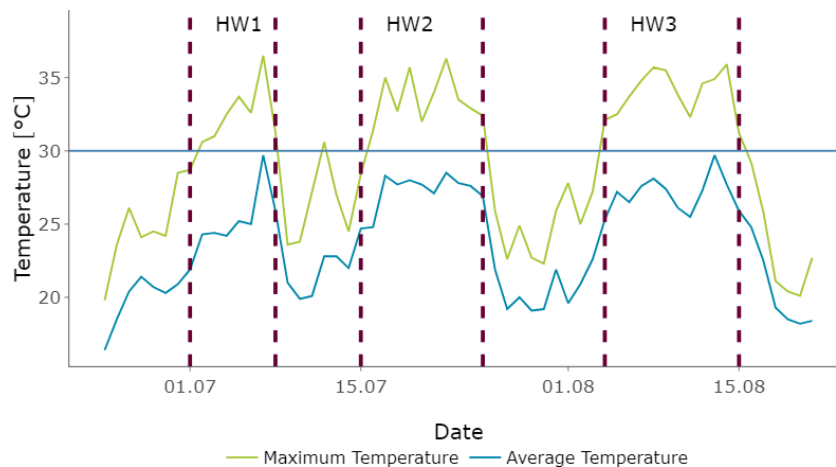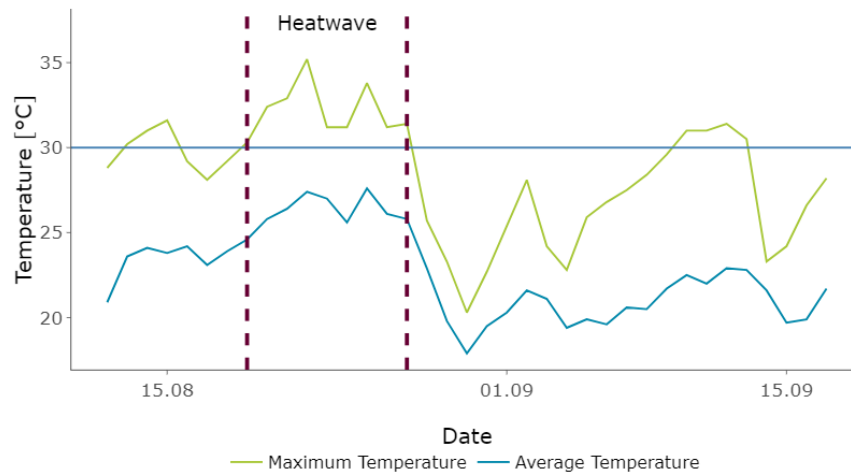
Abb. A-14: Maximum and average temperature in the time of the selected heatwave in 2023.
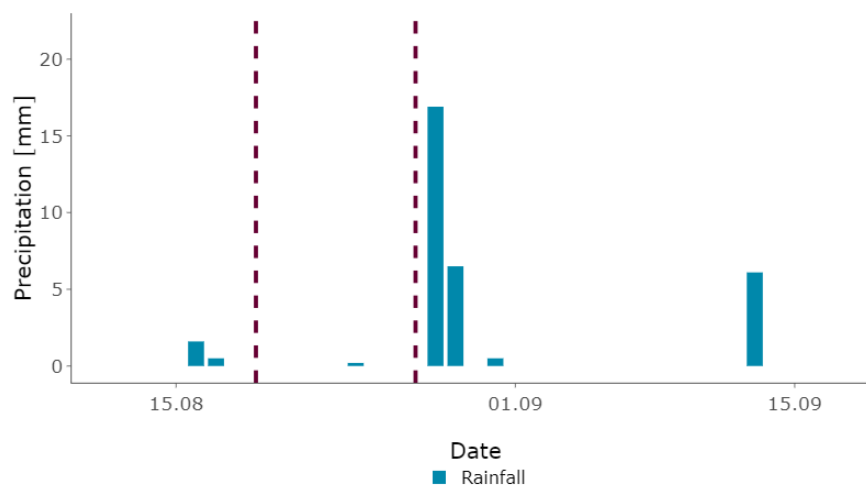
Abb. A-15: Precipitation in the time of the selected heatwave in 2023.

The water balance before the heatwave in 2023 is positive (0.8 to -1.03). This changes during the heatwave (-0.39 to -0.04). After the heatwave, the SPEI 30 index indicates even more dryer conditions (-2.1 to -1.26), although rainfall events occurred.

A-5.2.5   Heatwaves 2024

The heatwaves in 2024 took place in mid-August and beginning of September. This one is the latest heatwave of the eight selected ones. The maximum temperature is both times approximately 35°C, with average temperature during the heatwaves between 25°C and 28°C. Between both heatwaves, a single day of over 30°C occurred, and the average temperature stayed over 20°C, whereas a temperature drop occurred after HW 8. Daily maximum temperatures decreased up to 10°C (Abb. A-16:). Looking at the precipitation during the whole period, we can observe singular precipitation events before and during HW 7, then a dry period until the end of HW 8. Afterwards, heavier rainfall events occurred relating to the drop in temperature (Abb. A-17:).
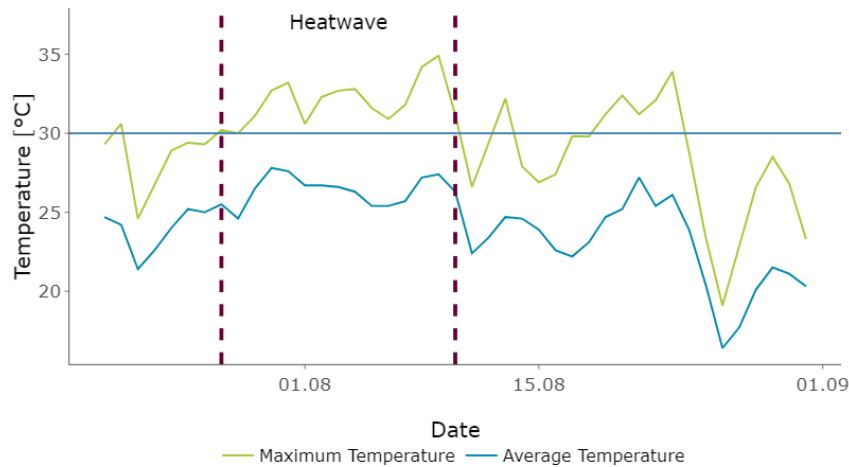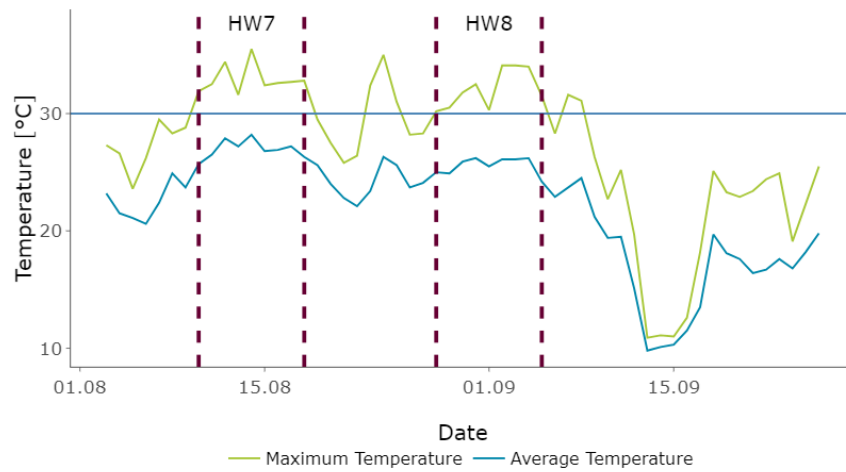
Abb. A-16: Maximum and average temperature in the time of the selected heatwaves in 2024.
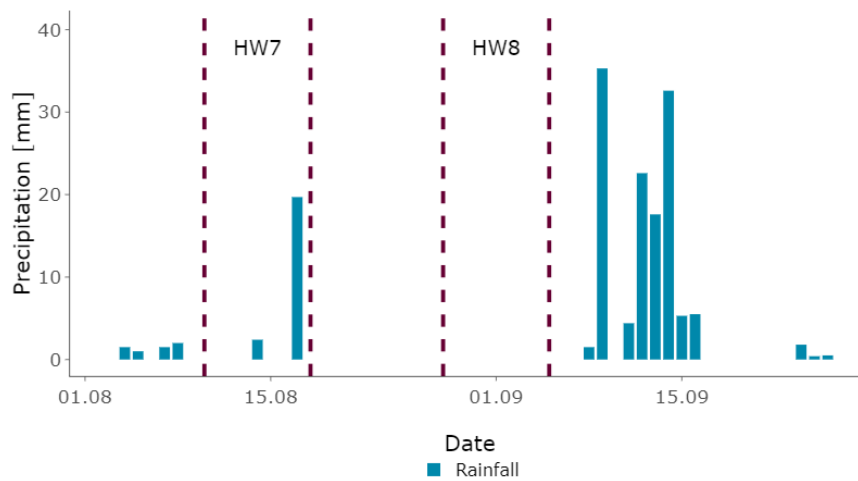
Abb. A-17: Precipitation in the time of the selected heatwaves in 2024.

For the time before the selected heatwaves in 2024, the SPEI30 index shows dry conditions (-1.2 to -1). During the heatwave, the conditions remain dry (-1.32 to-0.91). Afterwards, related to the increase in precipitation, the water balance is positive (1.13 to 1.43).

A-6 Analysing the impacts of heatwaves using thermal data

In this study, Land Surface Temperature (LST) was retrieved from Landsat 8 Collection 2 Level-2 data (LC08/C02/T1_L2) over the region encompassing the AOI. We focused on the thermal infrared sensor band ST_B10, which provides brightness temperature at 100-meter resolution. To maintain consistency with surface reflectance bands, we resampled to 30 meters throughout processing.

Only daytime scenes with high solar elevation (greater than 40°C) were included to avoid morning or evening bias. Cloud-contaminated pixels were removed using bitmask filters from the QA_PIXEL band, specifically targeting cloud and cloud shadow flags. Even with these filtering, some artifacts, such as holes or missing pixels still occur as they are inherent to the L8 Collection-2 Level-2 data. These arise primarily from the conservative cloud and cloud-shadow masking applied via the QA_PIXEL band done by the Landsat data team, which often removes valid pixels near clouds or their edges. While using image composites (e.g., median) helps reduce the visual impact of these gaps, persistent atmospheric interference or systematic artifacts may still lead to small holes in the final LST output. These are considered known limitations of the L2 surface temperature product and were accounted for during the interpretation of spatial and temporal patterns.

Brightness temperature from the thermal band was scaled using standard coefficients and then converted to LST in degrees Celsius. Emissivity correction was applied using an NDVI-based approach. NDVI was computed from the red (SR_B4) and near-infrared (SR_B5) bands. Fractional vegetation cover (FV) was estimated from NDVI, and surface emissivity was derived using a simple linear formula. The final LST formula was corrected for emissivity and atmospheric effects using the Planck equation (Jiménez-Muñoz & Sobrino, 2003). We then calculated the mean LST per polygon per date and generated time series grouped by land cover class (CLC_CODE). Unrealistic temperature values (below -10°C or above 60°C) were filtered out to avoid skewed results. The output is a set of interpretable thermal signatures across land cover types during the summer season.

The resulting maps and graphs below include both static LST maps for specific heatwave windows (2015, 2018, 2022–2024) and the LST time series (2015–2024) that reveal temporal dynamics across protected and non-protected areas and grouped by the CLC classes (Abb. A-18: to Abb. A-22:).
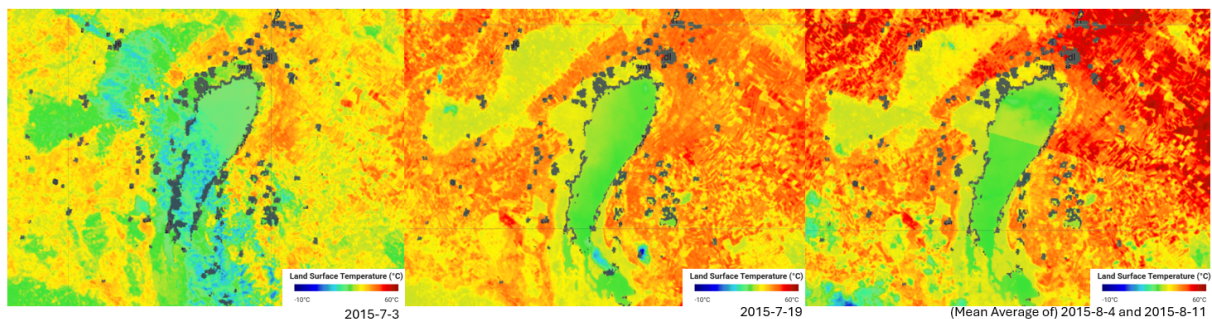
Abb. A-18: Land surface temperature in 2015 corresponding to the heatwave period on Abb. A-8.

(Average of) 2018-7-27 and 2018-8-3
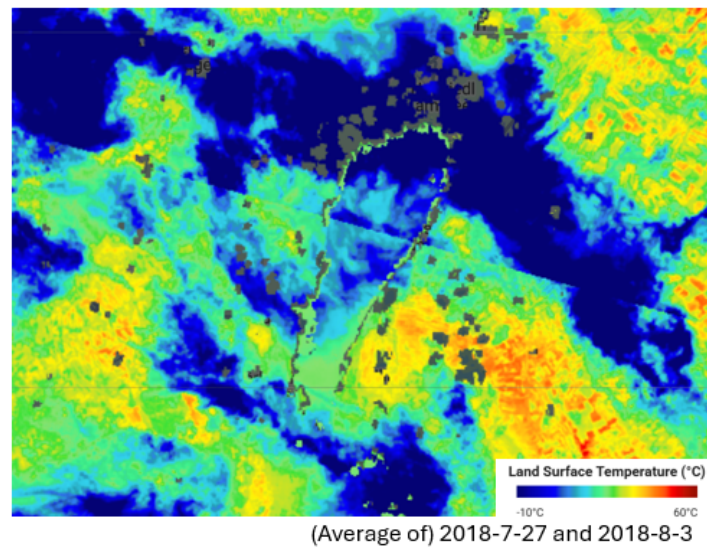
Abb. A-19: Land surface temperature in 2018 corresponding to the heatwave period on Abb. A-10.

2022-7-19
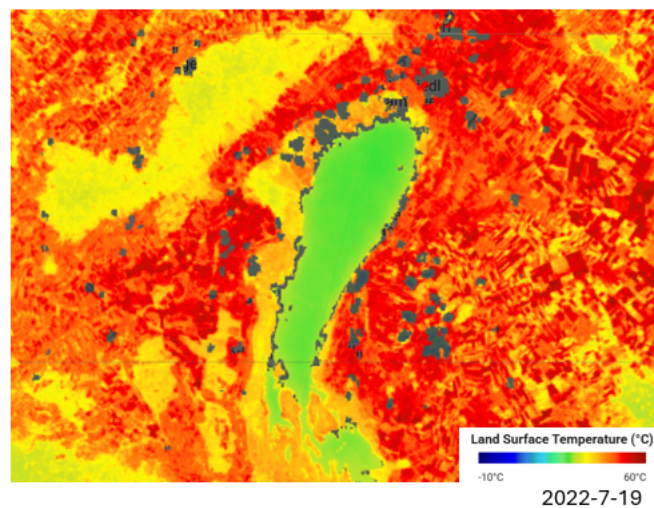
Abb. A-20: Land surface temperature in 2022 corresponding to the heatwave period on Abb. A-12

2023-8-26
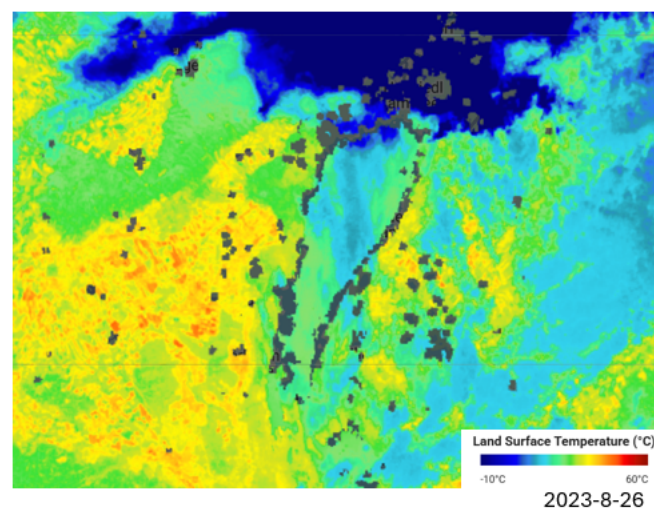
Abb. A-21: Land surface temperature in 2023 corresponding to the heatwave period on Abb. A-14
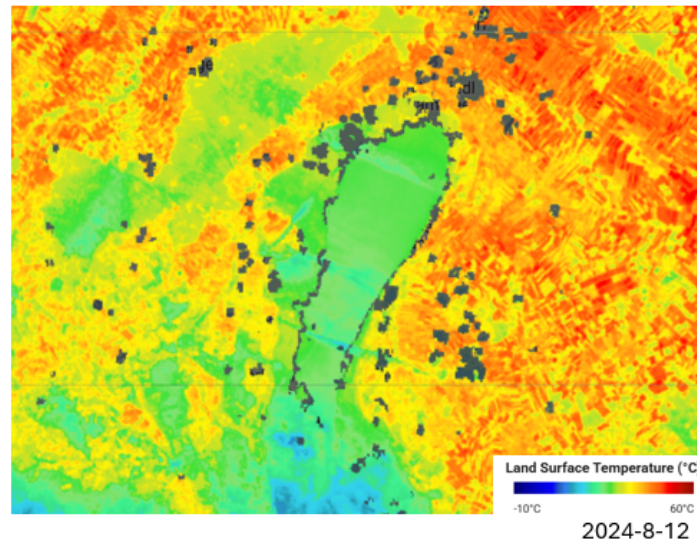
Abb. A-22: Land surface temperature in 2024 corresponding to the heatwave period on Abb. A-10 2016.

The resulting LST maps and LST time series show clear thermal responses during the eight selected heatwaves, with distinct peaks in 2015, 2022, and 2024 corresponding to periods of high maximum air temperature and negative SPEI30 values (indicating drought). For instance, the intense heatwave in July 2022 (Abb. A-20), is also captured in the LST maps as a widespread surface temperature spike across bare and agricultural areas. In contrast, years like 2018 and 2023 show milder thermal anomalies in both air and surface temperatures because of clouds, consistent with more moderate SPEI trends and scattered precipitation events.

Overall, the Landsat-based LST patterns reflect the temporal and spatial dynamics of heat stress in the region and reinforce the documented trends of more frequent, prolonged, and spatially extensive heatwaves in recent years.
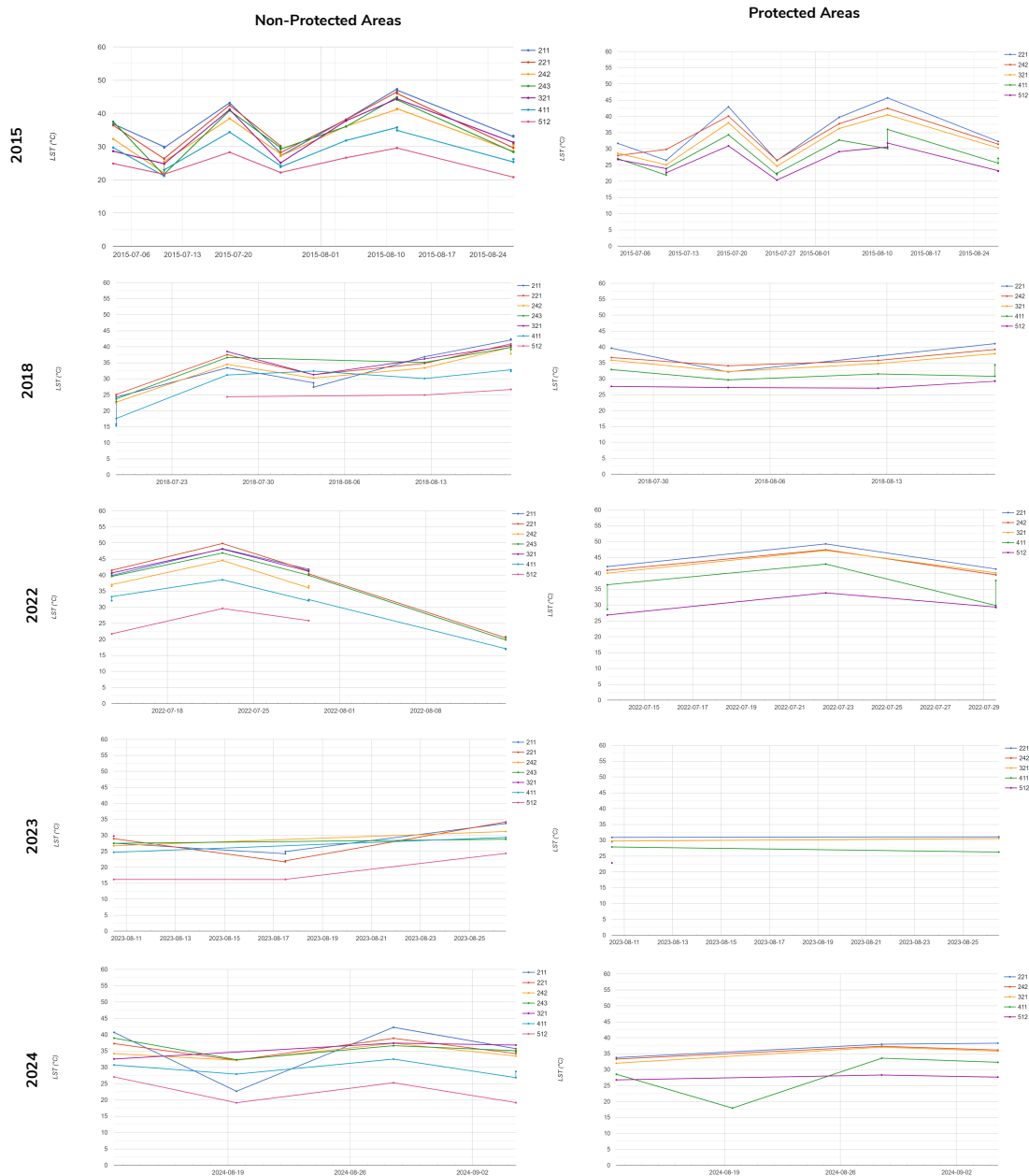
Abb. A-23: The time series of LST from 2015 to 2024 for non-protected areas and protected areas.

A-7 Impacts of heatwaves on the vegetation

To assess the impact of heatwaves on vegetation, we decided to look at different subareas in the study area. This allowed us to identify potential differences between protected and non-protected areas as well as the land cover classes (Tab. A-3:).

Tab. A-3: Corine Land Cover Classes (CLC) found inside the study area.

CLC Code	Label 11	Label 2	Label 3
211	Agricultural areas	Arable land	Non-irrigated arable land
221	Agricultural areas	Permanent crops	Vineyards
231	Agricultural areas	Pastures	Pastures
242	Agricultural areas	Heterogeneous agricultural areas	Complex cultivation patterns
243	Agricultural areas	Heterogeneous agricultural areas	Land principally occupied by agriculture, with significant areas of natural vegetation
311	Forest and semi natural areas	Forest	Broad-leaved forest
313	Forest and semi natural areas	Forest	Mixed forest
321	Forest and semi natural areas	Scrub and/or herbaceous vegetation associations	Natural grasslands
324	Forest and semi natural areas	Scrub and/or herbaceous vegetation associations	Transitional woodland-shrub
411	Wetlands	Inland wetlands	Inland marshes

For each of the selected subareas, we conducted time series analysis for several vegetation indices (Tab. A-4: and Tab. A-5:) and performed both a Kendall trend and a significance test. The indices were calculated using Google Earth Engine (GEE), and further statistical analysis was carried out in R (R Core Team, 2021). To reduce the influence of clouds, only S2 images with less than 10% cloud coverage were selected. The selection of indices was based on a literature review conducted within the StartClim Project HAGL (Streifeneder et al., 2023a, 2023b).

Tab. A-4: Vegetation indices for estimating plant health (Furlanetto et al., 2023; Ha et al., 2022; Sosa et al., 2021)

Vegetation Index - Plant Health	Description
Normalized Difference Vegetation Index (NDVI)	Indicator for plant density and plant health
Green Normalized Difference Vegetation Index (GNDVI)	Indicator for photosynthesis

Modified Soil-Adjusted Vegetation Index (MSAVI2)	Indicator for plant density and plant health at the beginning of phenology
Soil-Adjusted Vegetation Index (SAVI)	Soil-adjusted NDVI
Plant Senescence Radiation Index (PSRI)	Indicator for the aging process of leaves and seedlings
Enhanced Vegetation Index (EVI)	Indicator for leaf canopy area and density
Advanced Vegetation Index (AVI)	Indicator for change in plant health
Atmospherically Resistant Vegetation Index (ARVI)	Indicator for change in plant health – atmosphere-corrected
Leaf Area Index (LAI)	Indicator for leaf area
Modified Chlorophyll Absorption Ratio Index (MCARI)	Indicator for chlorophyll content

Tab. A-5: Vegetation indices for estimating water balance in plants (Furlanetto et al., 2023; Ha et al., 2022; Sosa et al., 2021)

Vegetation Index - Water Balance	Description
Moisture Stress Index (MSI)	Water content of the leaves
Normalized Difference Water Index (NDWI)	Indicator for water content in plants and soil

To avoid including information from correlating indices and ensure comparability between different land cover classes and areas, we applied a principal component analysis (PCA) for dimensionality reduction. Based on the PCA results, only the MSI, NDVI, SAVI, and PSRI indices were used in the subsequent analyses (Abb. A-24:).

StartClim2024.A
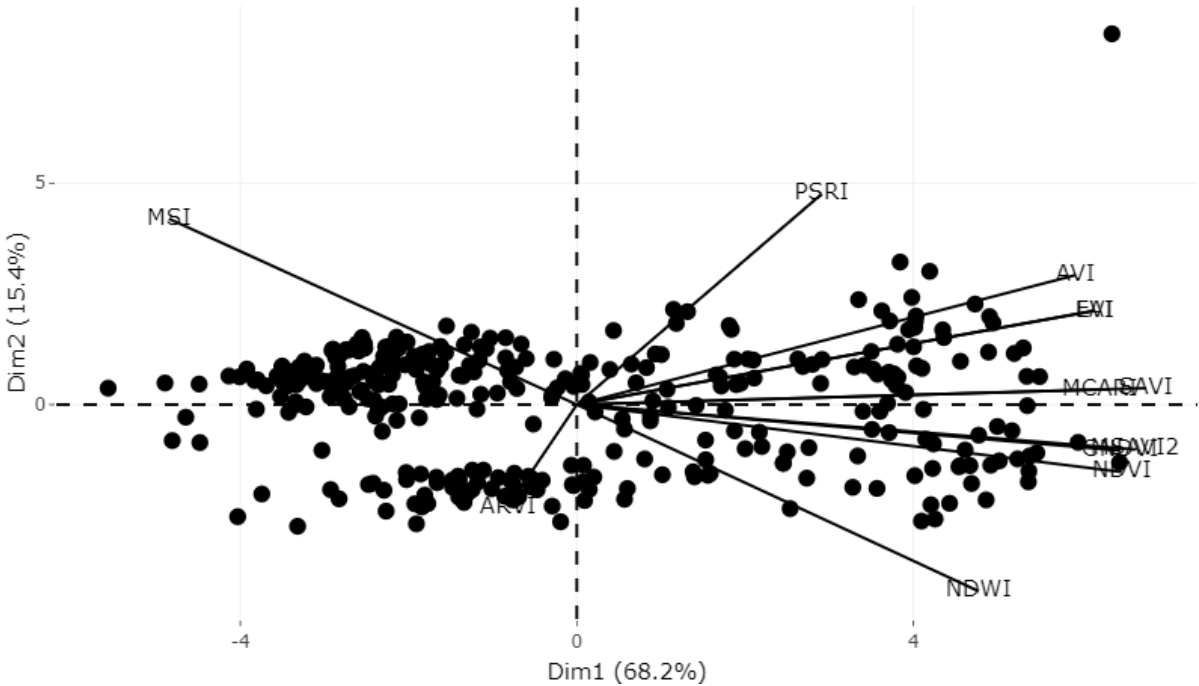
Abb. A-24: PCA - Biplot for the first two principal components to assess the relation between different indices.

To assess the impact of each heatwave on vegetation health, we compared the median values of each index before and after the heatwave events. The median was chosen to reduce the influence of outliers, which could have been caused by residual cloud effects. Furthermore, dates where more than 20% of a land cover polygon was covered by clouds were excluded to further reduce cloud-related biases (Abb. A-25:).
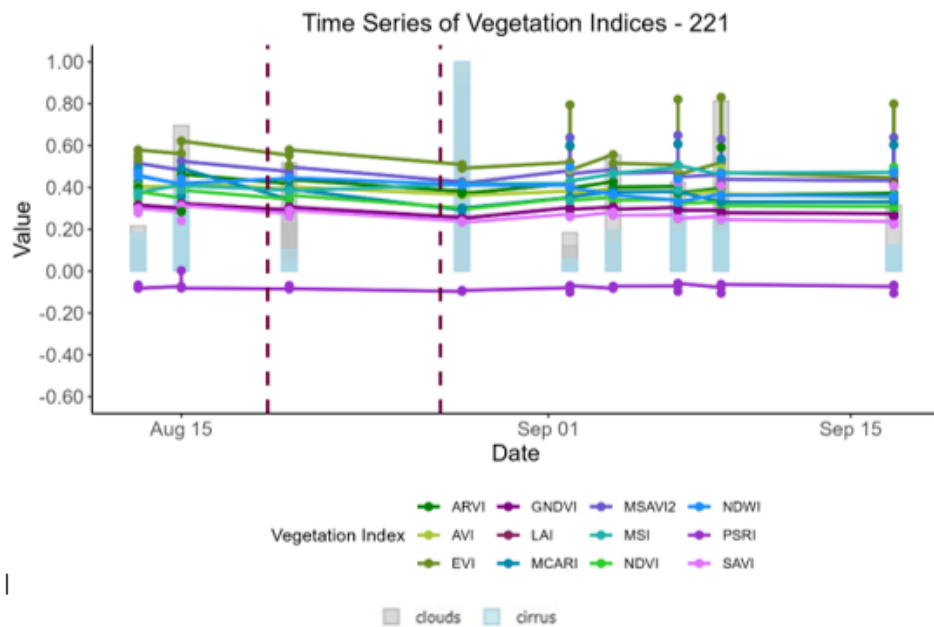
Abb. A-25: Time series of vegetation indices for land cover class 211 (Point 1) in 2023 for all indices. A noticeable influence of cloud cover is visible.

For comparing the impact of the selected heatwaves across subareas, we estimated the relative change per land cover class based on the observed variation in each index. To quantify the variability in vegetation response across indices, we calculated the range of change as the difference between the maximum and minimum percentage changes across all selected indices, when a significant trend ($p<0.05$) was observed. This metric captures the spread in index behaviour and provides insights into the effect of heatwaves on vegetation health. A larger range indicates a greater change in vegetation health, which can be either positive or negative; however, in our study, only negative changes were observed. This approach also enables better comparisons between subareas and individual heatwaves.

It is important to note that vegetation indices may decrease not only due to heatwaves but also because of clouds, harvesting, irrigation, or other natural disturbances. Therefore, we complemented our analysis with feedback from stakeholders and consideration of different subareas.

A-7.1 Vegetation health in the unprotected areas

We selected five different areas outside the national park (Abb. A-26:). Abb. A-26: provides an example of the development of vegetation indices from one week before to three weeks after the 2023 heatwave for the selected area Point 2. A decline in vegetation health is visible through a slight decrease over time for NDVI and SAVI and an increase for MSI.
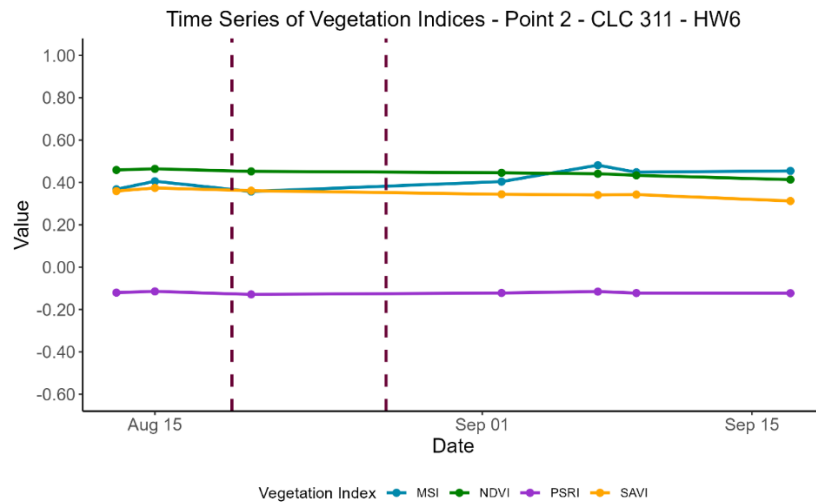
Abb. A-26: Example of a time series analysis for the different vegetation indices for the land cover class 311 for 2023 in Point 2.

The relative change in vegetation indices per CLC class and heatwave (Abb. A-27:) supports the overall assessment of vegetation health during the different heatwave events. Overall, we can see changes in the vegetation health during all heat waves as well as the different effects each heatwave had on the different land cover classes in the selected subareas. For example, class 411 in Point 4 appeared to be more affected than in other locations, and heatwave 4 seems to have more impact than the other heatwaves.
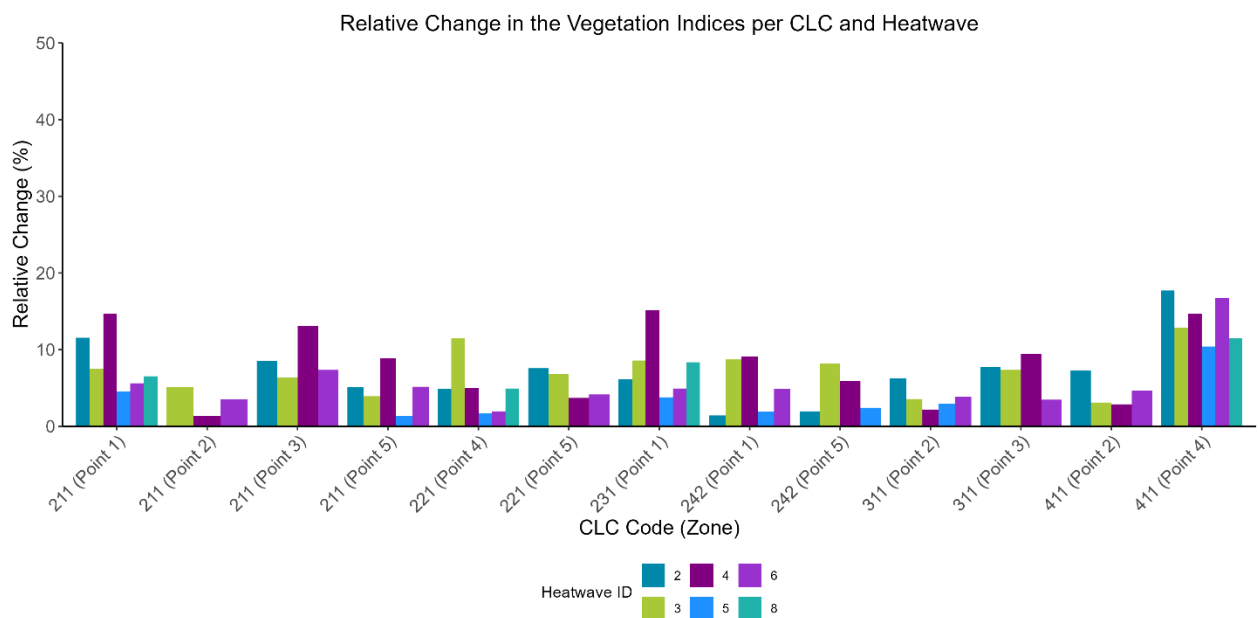
Abb. A-27: Relative changes in vegetation indices per CLC and heatwave for unprotected areas. For heatwave 1 and heatwave 7, not enough cloud-free images were available for the analysis. Not all observed changes have been significant; hence, points and land cover class are missing.

A-7.2 Vegetation health in the protected areas

The national park areas were separated into five different zones (Abb. A-1:). The zones were defined based on geographical location and vegetation. This allowed a better understanding of the impact of heatwaves on the protected areas in the study region.

Abb. A-28: shows an example of time series of vegetation indices for the vegetation class 411 in zone 3 for 2023. A decrease of NDVI and SAVI, as well as an increase of MSI and PSRI over time, indicates the reduction of plant health after the heatwave.
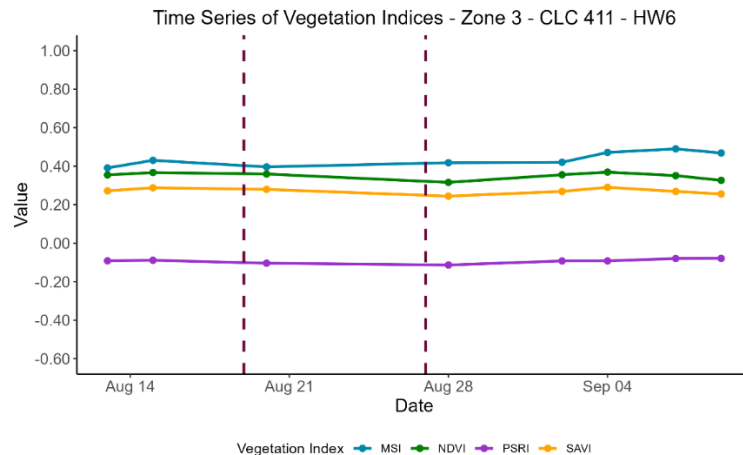
Abb. A-28: Example of a time series analysis for the different vegetation indices for the land cover class 411 for 2023 in Zone 3.

A closer analysis shows that each heatwave affects the land cover classes differently. In addition, differences can be observed between similar land cover types across different zones (Abb. A-29:). Overall, a decline in plant health following heatwaves is visible, likely caused by heat and water stress.
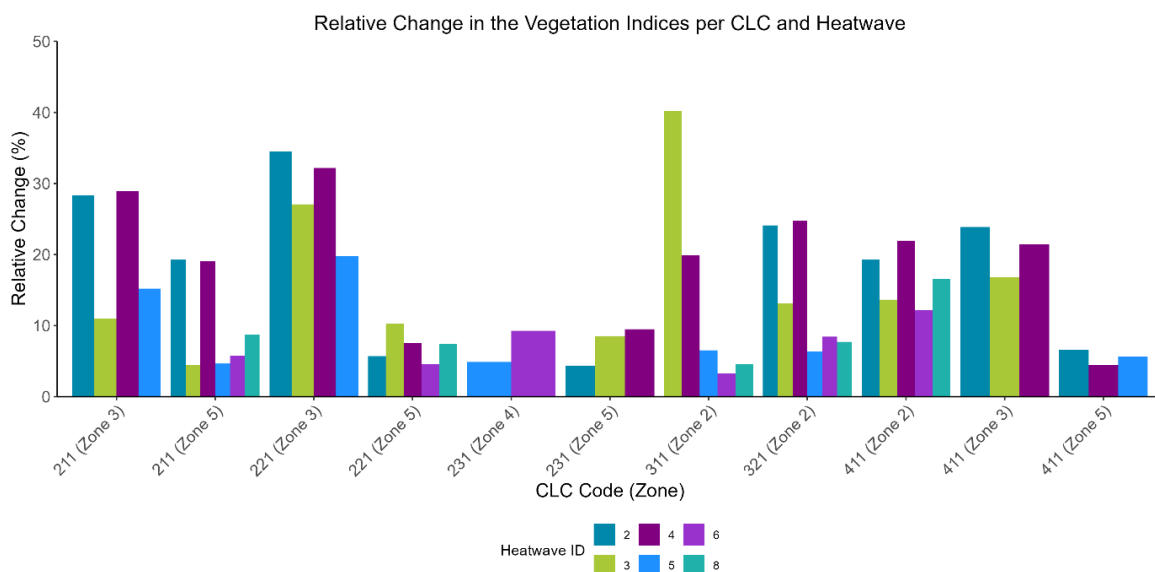
Abb. A-29: Relative changes in vegetion indices per CLC and heatwave for protected areas. For heatwave 1 and heatwave 7, not enough cloud-free images were available for the analysis. Not all observed changes have been significant; hence, zones and land cover class are missing.

A-8 Correlation between heatwaves, surface/water temperature and vegetation

This chapter reports about the correlation between heatwaves, surface/water temperature and vegetation health. Concluding from the results in chapter A7, heatwaves have a different impact on the vegetation health, varying between heatwaves, location and land cover class.

When comparing the relative change in vegetation indices per heatwave and CLC class (Abb. A-27: & Abb. A-29:), we observe that the impact of heatwaves differs between protected and non-protected areas. Overall, protected areas appear to be more affected by heatwaves than non-protected areas. This difference can be partly explained by the distribution of land cover types: non-protected areas are predominantly agricultural, while protected areas consist largely of grassland, forest and marshland. Agricultural areas in non-protected regions seem less affected, likely due to the use of irrigation and other adaptation measures that help mitigate heat stress. In contrast, forests and marshlands in protected areas show stronger vegetation index changes, suggesting a greater sensitivity to heatwave events.

However, these results are only first tendencies which need to be further analysed. Part of this is the stakeholder feedback received throughout the project (A-9.1); another part would be a larger follow-up project, incorporating longer time-series events and more detailed analysis of vegetation change caused by other factors that could potentially influence the current results as well.

A-9 Validation

Originally a field trip was planned to validate our results, however due to tragically events we were not able to conduct this trip. Instead we conducted several mitigation measures to validate our results and gather feedback from stakeholders.

A-9.1 Feedback from the UNESCO Heritage Association (17.6.2025)

In the course of an online meeting, we presented the results of our project to the UNESCO Heritage Association. Our findings may be of interest for assessing the attributes of the UNESCO Heritage site. A proposal for a follow-up project focusing more on this aspect has already been submitted. Furthermore, the meeting provided interesting insights and ideas for further research.

From their experience, the northern part of the Neusiedler See generally appears to be hotter, and heatwaves last longer compared to the southern part. This aligns with some of our observations regarding vegetation health. Moreover, referring to the thermal data, they also suggest an influence of the local topography - on the west side of the lake, a small, forested mountain range could cause a cooling effect, while the east side is flat. Researching this effect would go beyond the scope of the current project, but would be of interest for future projects.

Additionally, they reported a reduction in the number of small salt lakes in recent years, as they have dried out permanently due to dry conditions (we received similar information from the National Park). Moreover, other projects are researching ways to increase the heat resistance of marshlands, as well as focusing on the public dissemination of scientific findings (Verein Zukunft Neusiedler See).

A-9.2 Local measurements in Salzburg (19.6.2025)

To support the use and interpretation of EO–derived LST data, here we report a validation strategy combining field measurements (A-9.2), reference to existing high-resolution thermal data collection (airborne) campaigns (A-9.3), and cross-checks with other satellite-based thermal products (A-9.4). These efforts, while scaled to available resources, ensure that the derived thermal signals used to process over the Neusiedler See region are not only visually interpretable but also physically validated.

We conducted a small-scale sample measurements at representative land cover types (e.g., soil, sunlit grass, shaded grass) around the Salzachsee area in Salzburg (Abb. A-30:) using the Testo 905-T2 probe (for surace temperature), a FLIR thermal camera (for thermal images), and a Kestrel weather meter (for air temperature, relative humidity, heat index, etc.).
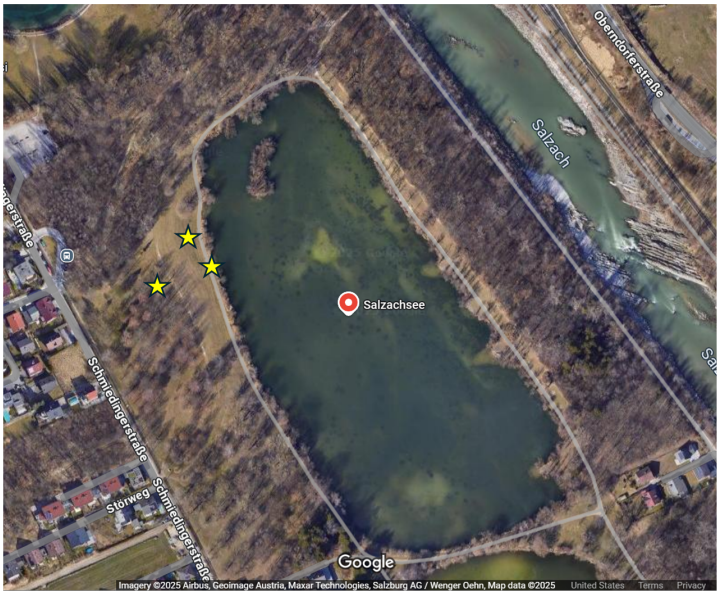
Abb. A-30: Study area for the sample field measurement: Salzachsee. The yellow points correspond to the sample points in Table A-6.

These tools allowed us to collect surface temperature measurements over selected materials at different times under varying sun exposure (see Tab. A-6). Abb. A-31:**Fehler! Verweisquelle konnte nicht gefunden werden.** gives two examples of the FLIR Thermal Image Report for sample sites over the Salzachsee region. The purpose of this exercise was not statistical robustness, but to test instrument performance and assess internal consistency across sensors (Testo, FLIR, Kestrel). The results also serve as a qualitative reference point for interpreting relative temperature patterns in Landsat 8 LST products, as previously reported. While absolute values from in-situ probes and relative values from satellite data are not directly comparable due to scale, emissivity assumptions, and measurement value, the observed temperature contrasts across land cover types (e.g., dry soil vs. shaded grass) follow similar trends in both datasets, supporting confidence in the EO-derived relative thermal signal.
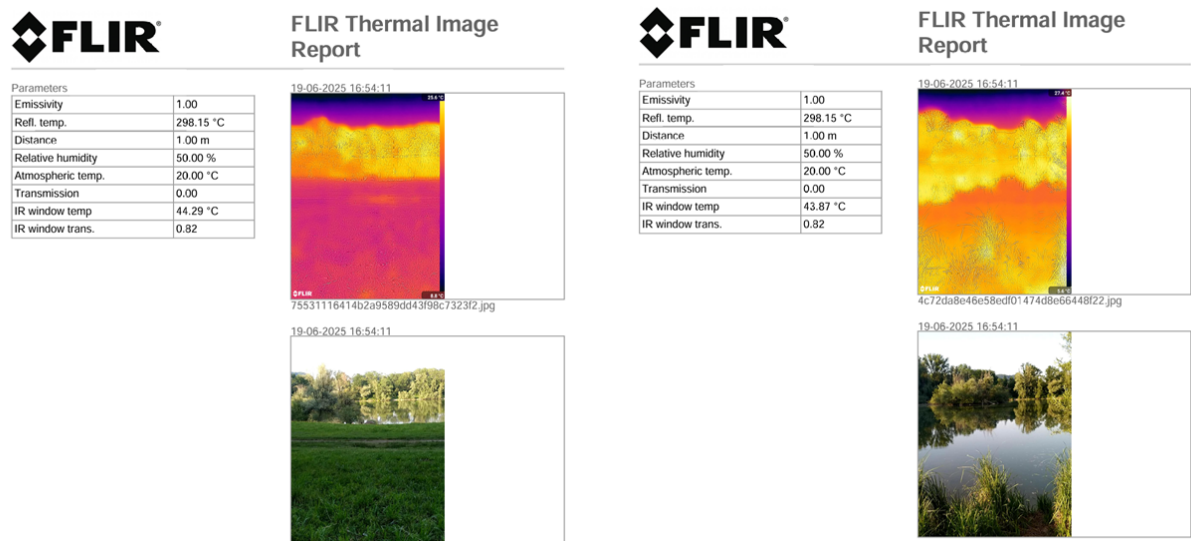
Abb. A-31: Thermal image samples over the sample site in Salzburg.

Surface temperatures were recorded across different land cover types (e.g., sunlit grass, shaded grass, dry soil with rocks) on Tab. A-6, at close intervals around 18:50–19:10 CEST. Values ranged from 32.8 °C for dry sun-exposed soil to 25.0 °C for shaded grass. The FLIR camera confirmed spatial consistency with the Testo readings ($\Delta < 0.5$ °C), while air temperature measured by the Kestrel ranged from 26.7 °C to 30.1 °C, providing context. These results not only validate instrument consistency but also reflect realistic surface heterogeneity as driven by microclimatic exposure. Notably, the field acquisition took place on 19 June 2025, closely matching the date of the ECOSTRESS scene processed (A-9.4) for Neusiedler See, providing a relevant temporal overlap.

Tab. A-6: Sample Surface Temperature Measurement with the Testo 905 probe for different materials.

No.	Location	Image	Class Type	Surface Temp#1	Surface Temp #2	Surface Temp #3
1	47.835401, 13.018428		Dry soil with rocks (direct sun)	32.8 C @6:53pm	31.1 C @ 6:59pm	30.7 C @7:05pm
2	47.835650, 13.018160		Grass (direct sun)	26.8 C @6:51pm	26.4 C @ 6:57pm	25.7 C @7:04pm
3	47.835281, 13.018007		Grass (under tree shade)	25.2 C @6:55pm	25.1 C @7:02pm	25.0 C @7:08pm

-
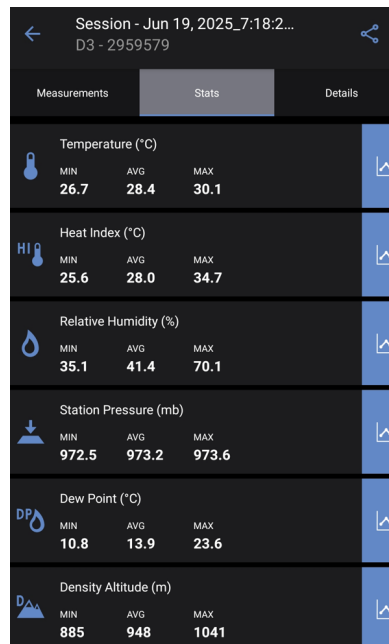
Abb. A-32: 1Kestrel DROP 3 log of air temperature, heat index, humidity, and other parameters, reporting the minimum and maximum values during the observation period.

A-9.3 2. Insights from the PROMETHEUS Project

To contextualize these field observations, we are referencing the thermal validation work done in the PROMETHEUS project (ongoing, FFG project), where a comprehensive setup combining aircraft-based thermal imaging (1m resolution), in-situ stations using the same Testo 905-T2 probe across multiple surfaces (e.g., water, grass, soil, asphalt), and synchronized day-night surveys were used to validate and support satellite LST mapping. The PROMETHEUS thermal validation campaign showed differences between in-situ and airborne thermal data ranging from 5°C to over 10°C, depending on surface type and conditions.

Abb. A-33: 2Kestrel DROP 3 log of air temperature, heat index, humidity, and other parameters, reporting the minimum and maximum values during the observation period.
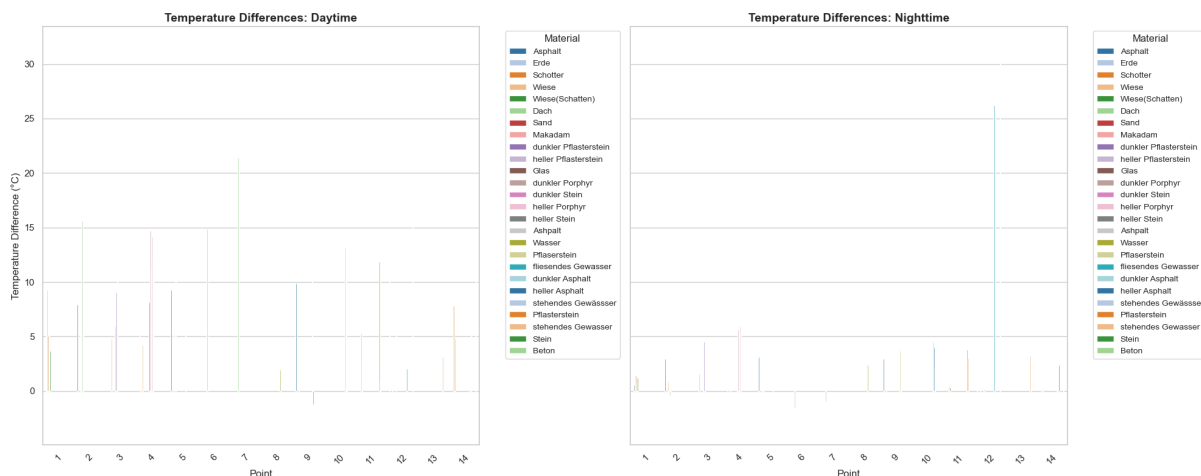
These insights illustrate the scale mismatch and variability of values expected when comparing point-based ground truth to EO-derived LST at resolutions like Landsat (100 m) or ECOSTRESS (70 m). Our field protocol follows this same logic, though scaled down, and confirms that such differences are not only expected but also quantifiable.

A-9.4   Derivation of LST using other satellite imagery

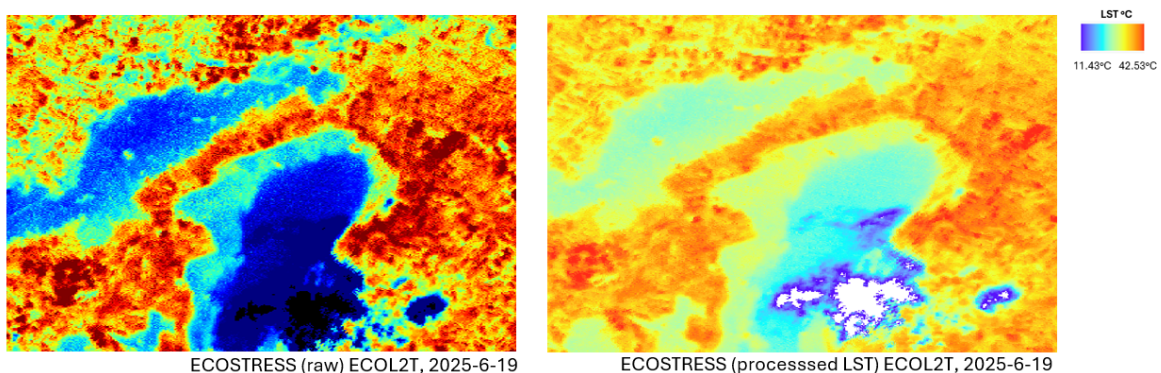ECOSTRESS (raw) ECOL2T, 2025-6-19   ECOSTRESS (processsed LST) ECOL2T, 2025-6-19

Abb. A-34: Raw and processed ECOSTRESS (LST) dataset over Neusiedler See. The image tile covering the majority of the region was selected for processing.

The ECOSTRESS (ECOsystem Spaceborne Thermal Radiometer Experiment on Space Station) mission provides high-resolution thermal infrared data from the International Space Station (ISS), enabling the retrieval of LST at ~70 m spatial resolution. For this analysis, the ECOSTRESS Level 2 temperature product (ECO_L2T_LSTE, V002) was used, which provides LST as scaled 16-bit values in Kelvin, accompanied by quality and view geometry layers. Since ECOSTRESS operates from the ISS, its temporal revisit is irregular depending on latitude and orbital scheduling, with occasional multi-day gaps between acquisitions over the same location.

We processed ECOSTRESS thermal data for Neusiedler See to derive higher-resolution LST. The raw data was subsetted via AppEEARS platform to a custom AOI over Neusiedler See (Austria), and exported. In the processing workflow, the LST band was scaled using the official factor (0.02) and converted to Celsius. Invalid or low-quality pixels were masked using the associated LST quality control (QC) bitmask. The image on the left of Abb. A-34:shows the raw LST scene for 2025-06-19, with artefacts and cloud-contaminated pixels still visible. The right panel shows the processed dataset after masking and color-normalization, revealing more accurate spatial gradients. Land-water contrasts, especially around the and shallow areas of the lake, are more clearly resolved in the processed map. Temperature values range from approximately 11.4°C to 42.5°C, with cooler zones over open water and elevated values over dry surfaces especially on built-up areas. The average temperature observed was around 30.51°C. On Abb. A-35:, the boxplot for the LST values report a temperature range from 27.37 °C to 34.11 °C, with a median LST of 31.61 °C across the scene. Most surface temperatures cluster within this interquartile range, while a few lower outliers (around 13.4 °C) likely correspond to cloud-contaminated or masked water pixels. The distribution reflects typical early summer heating patterns, with elevated temperatures over dry surfaces and cooler zones over shaded or water-covered areas.
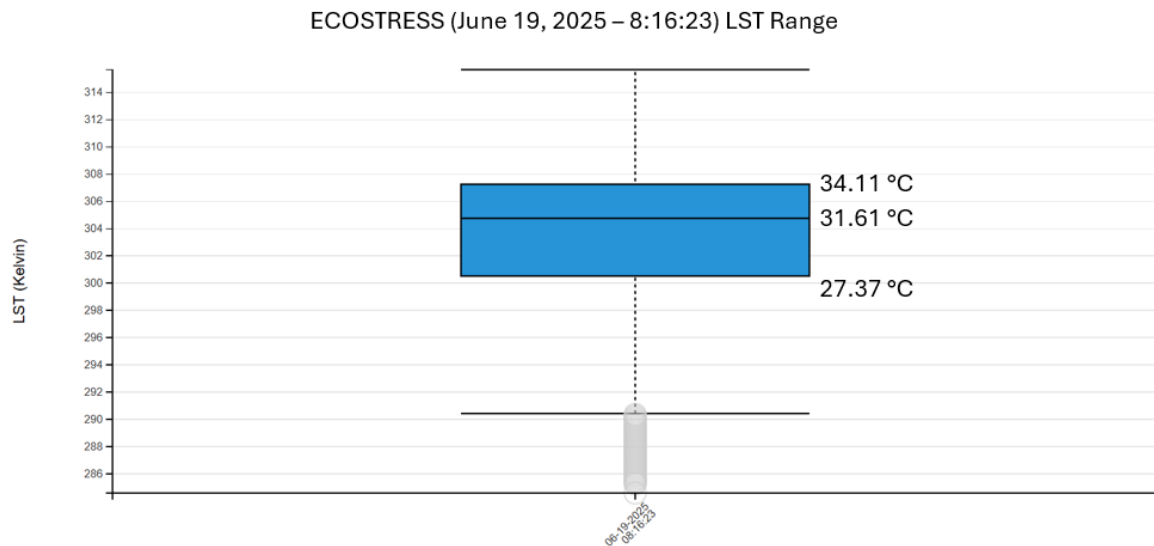
Abb. A-35: Pixel values statistics of the ECOSTRESS image for June 19, 2025.

The field-to-satellite correspondence, especially the temporal match with ECOSTRESS data, supports confidence in our LST interpretation. For further lake-specific validation or climatology, products such as ESA-CCI Lakes - Lake Water Surface Temperature (LWST)(Copernicus Climate Change Service & Climate Data Store, 2020) can be explored for long-term trends in lake surface temperature derived from multiple satellite missions (e.g., ATSR-2, MODIS, AVHRR, Sentinel- 3 SLSTR) spanning from 1995–2022.

A-10   Dissemination and Application potential

A number of different dissemination activities took place. This included the presentation of first results at the Austrian Climate Day (Österreichischer Klimatag) in Innsbruck in April 2025:

Streifeneder, V., Arellano, C., Dabiri, Z., Hölbling, D., 2025. Analyse der Auswirkungen von Hitzeperioden auf die Oberflächen-und Wassertemperatur in der Region Neusiedler See -Seewinkel mit thermischen Satellitendaten. 25. Österreichischer Klimatag, Innsbruck, Austria, 23-25 April. https://ccca.ac.at/fileadmin/00_DokumenteHauptmenue/05_Veranstaltungen/Klimatag/2025/Vortrags folien/wiss.sessions/V03_Streifeneder.pdf

In addition, we exchanged ideas with experts from academia at the EGU General Assembly 2025 in Vienna. The conferences were also used to receive feedback, establish new contacts, and discuss possible further research and collaboration opportunities.

The findings from the project were also partly integrated into teaching at the university, particularly the analysis of the thermal data and the processing using the GEE.

Further dissemination activities included posting information about the project on the website of the research group "Risk, Hazard & Climate" at the Department of Geoinformatics - Z_GIS, (https://www.plus.ac.at/geoinformatik/research/research-areas/risk-hazard-climate/projects/?lang=en) and the research portal of the University of Salzburg (PLUS Research).

An important aspect was the regular exchange with stakeholders to assess the application potential of our research. In particular, we conducted several online meetings with the National Park Neusiedler See - Seewinkel and the Verein Welterbe Neusiedler See. During these meetings (initial) project findings were presented and discussed, feedback collected, application and exploitation opportunities evaluated, and potential future collaboration discussed. In addition, HOT facilitated to establishment of further contacts, for example, we had meetings with Geosphere Austria and the TU Vienna for scientific and data exchange and initiated a collaboration with the Chair of Climate Geography at the University of Freiburg and the company Termatics.

The experiences from HOT enabled us to identify a range of future application fields including regional and local planning, environmental conservation and nature protection, agriculture, and sustainable tourism. For example, future exploitation could be an intensified collaboration with the National Park Neusiedler See - Seewinkel to provide them with additional information to support their efforts in nature protection and sustainable tourism, and with the Verein Welterbe Neusiedler See to provide relevant information about developments and changes in the UNESCO World Heritage region. By relying on freely available satellite data and considering the steadily increasing temporal and spatial resolutions of optical, radar and thermal satellite sensors, a high potential for upscaling to other and larger regions in future research is given, potentially resulting in a future Earth observation-based monitoring solution for assessing the impacts of extreme weather events.

A-11   Conclusion and Outlook

In the HOT project, we addressed three research questions. The first one referred to the advantages of using thermal EO data to identify the impact of heatwaves on surface temperature. In particular, thermal EO data can help obtain surface temperature information for large areas. However, due to the comparatively coarse resolution, the information can only be used for estimating trends and gaining a general overview. In-situ measurements and high-resolution thermal data are more suitable for small-scale analyses.

Second, we assessed the impact of heatwaves on protected and non-protected areas based on Sentinel-2 and Corine Land Cover data. It was possible to observe differences in plant health before and after a heatwave, as well as variations between protected and non-protected areas for the same land cover type. However, more detailed analyses are needed to gain a deeper understanding of the effects of heatwaves on vegetation and the influence of conservation measures across different land cover types. In particular, the resolution of the land cover data did not allow for detailed analysis at a smaller scale. Nevertheless, we were able to identify certain trends. The limited scope of this project did not allow us to explore these findings further, but the results demonstrate the potential of the approach. Therefore, future projects could use more detailed land cover maps and extend the observation period, for instance, by applying spectral-temporal metrics to create a robust reference dataset for comparing observed vegetation changes.

Finally, the role of protected areas in adapting to heatwaves is difficult to estimate and requires further research. According to interviews with our stakeholders, the protected area of the National Park includes ecosystems belonging to a warm climate. However, recurring heatwaves can still pose an ongoing threat to flora and fauna, for instance, by causing the permanent drying out of salt lakes. In the context of tourism, the area offers a broad spectrum of recreational activities, even during heatwaves, and tourism numbers have not declined (UNESCO Heritage Association – personal interview).

A-12   References

Amon, C. (n.d.). Das Schutzgebiet Neusiedler See- Seewinkel: Ökologie, Gefährdungen, Schutzstatus. https://www.naturschutzbund-burgenland.at/wissen/schutzgebietneusiedlerseeseewinkeloekologiegefaehrdungschutzstatus

Chimani, B., Heinrich, G., Hofstätter, M., Kerschbaumer, M., Kienberger, S., Leuprecht, A., Lexer, A., Peßenteiner, S., Poetsch, M. S., Salzmann, M., Spiekermann, R., Switanek, M., & Truhetz, H. (2016). Endbericht ÖKS15 – Klimaszenarien für Österreich - Daten - Methoden - Klimaanalyse. https://hdl.handle.net/20.500.11756/06edd0c9

Copernicus Climate Change Service, & Climate Data Store. (2020). Lake surface water temperature from 1995 to present derived from satellite observation. Copernicus Climate Change Service (C3S) Climate Data Store (CDS). https://doi.org/10.24381/cds.d36187ac

Crocetti, L., Forkel, M., Fischer, M., Jurečka, F., Grlj, A., Salentinig, A., Trnka, M., Anderson, M., Ng, W.-T., Kokalj, Ž., Bucur, A., & Dorigo, W. (2020). Earth Observation for agricultural drought monitoring in the Pannonian Basin (southeastern Europe): current state and future directions. Regional Environmental Change, 20(4), 123. https://doi.org/10.1007/s10113-020-01710-w

European Environmental Agency. (2018). CORINE Land Cover (20.01). European Environmental Agency. https://doi.org/https://doi.org/10.2909/960998c1-1870-4e82-8051-6485205ebbac

Furlanetto, J., Dal Ferro, N., Longo, M., Sartori, L., Polese, R., Caceffo, D., Nicoli, L., & Morari, F. (2023). LAI estimation through remotely sensed NDVI following hail defoliation in maize (Zea mays L.) using Sentinel-2 and UAV imagery. Precision Agriculture, 24(4), 1355–1379. https://doi.org/10.1007/s11119-023-09993-9

GeoSphere. (2024). Klimaindizes v2.1 Jahresdaten (2.1). GeoSphere. https://doi.org/https://doi.org/10.60669/g0yn-ws14

GeoSphere. (2025a). Stationsdaten. GeoSphere. https://data.hub.geosphere.at/group/stationsdaten

GeoSphere. (2025b). VIOLA-Unwetterchronik. GeoSphere. https://www.zamg.ac.at/cms/de/klima/klima-aktuell/unwetterchronik/?jahr=2016&monat=1

GeoSphere. (2025c). WINFORE v2.1 (2.1). GeoSphere. https://doi.org/https://doi.org/10.60669/f6ed-2p24

Ha, T., Shen, Y., Duddu, H., Johnson, E., & Shirtliffe, S. (2022). Quantifying Hail Damage in Crops Using Sentinel-2 Imagery. Remote Sensing, 14, 951. https://doi.org/10.3390/rs14040951

Jiménez-Muñoz, J. C., & Sobrino, J. A. (2003). A generalized single-channel method for retrieving land surface temperature from remote sensing data. Journal of Geophysical Research: Atmospheres, 108(D22). https://doi.org/10.1029/2003JD003480

Li, Z.-L., Tang, B.-H., Wu, H., Ren, H., Yan, G., Wan, Z., Trigo, I. F., & Sobrino, J. A. (2013). Satellite-derived land surface temperature: Current status and perspectives. Remote Sensing of Environment, 131, 14–37. https://doi.org/10.1016/j.rse.2012.12.008

Nationalpark Neusieder See Seewinkel. (2025). Natur und Forschung. https://nationalparkneusiedlersee.at/de/nationalpark/

R Core Team. (2021). R: A Language and Environment for Statistical Computing. https://www.r-project.org/

Richter, K., Rischbeck, P., Eitzinger, J., Schneider, W., Suppan, F., & Weihs, P. (2008). Plant growth monitoring and potential drought risk assessment by means of Earth observation data. International Journal of Remote Sensing, 29(17–18), 4943–4960. https://doi.org/10.1080/01431160802036268

Sosa, L., Justel, A., & Molina, Í. (2021). Detection of Crop Hail Damage with a Machine Learning Algorithm Using Time Series of Remote Sensing Data. Agronomy, 11(10), 2078. https://doi.org/10.3390/agronomy11102078

Streifeneder, V., Hölbling, D., & Dabiri, Z. (2023a). Auswirkungen von Hagelereignissen auf die Landwirtschaft: Eine fernerkundungsbasierte Analyse von Hagelschäden im Kontext des Klimawandels (HAGL)No Title (Endbericht von StartClim2022.E in StartClim2022: Schlüsselmaßnahmen, Messbarkeit Und Notfallszenarien). Auftraggeber: BMK, BMWFW, Klima- und Energiefonds. https://startclim.at/fileadmin/user_upload/StartClim2022/StCl22.E_lang.pdf

Streifeneder, V., Hölbling, D., & Dabiri, Z. (2023b). Impact of hail events on agriculture: A remote sensing-based analysis of hail damage in the context of climate change. EGU General Assembly 2023, EGU23-2551. https://doi.org/https://doi.org/10.5194/egusphere-egu23-2551

Tourismusverband Nordburgenland. (n.d.). Unesco Welterbe Region Fertő-Neusiedler See - Vielfalt am Steppensee. https://www.neusiedlersee.com/erleben/kultur-brauchtum/unesco-welterbe-region-neusiedler-see

Wegler, M., & Kuenzer, C. (2024). Potential of Earth Observation to Assess the Impact of Climate Change and Extreme Weather Events in Temperate Forests—A Review. Remote Sensing, 16(12), 2224. https://doi.org/10.3390/rs16122224

Zulka, K., Oberleitner, I., Baumgartner, C., Diry, C., Grabenhofer, H., Gross, M., Weber, A., & Schindler, S. (2022). Gefährdungsfaktoren und Schutzgebietsmanagement im Klimawandel. Verhandlungen Der Zoologisch-Botanischen Gesellschaft in Wien. Frueher: Verh.Des Zoologisch-Botanischen Vereins in Wien. Seit 2014 "Acta ZooBot Austria," 158, 49–80.